A DC Link Sensor-Less Voltage Balancing Technique for Cascaded H-Bridge Multilevel Converters With Asymmetric Selective Harmonic Current Mitigation-PWM

Amirhossein Moeini, *Student Member, IEEE* and Shuo Wang, *Senior Member, IEEE*

***Abstract*—A grid-tied cascaded H-bridge (CHB) converter with low frequency modulation techniques needs to meet power quality standards. At the same time, the effects of grid voltage harmonics on CHB converter's current harmonics must be considered in the modulation techniques. Furthermore, the dc link voltages of grid-tied converters need to be regulated. In this paper, an asymmetric selective harmonic current mitigation-pulse width modulation (PWM) (ASHCM-PWM) technique is used to meet the current harmonic limits of a power quality standard with the effects of grid voltage harmonics considered in the equation set of its optimization process. A voltage balancing technique based on the average power of each cell is derived to regulate the dc link voltages of the CHB converters without using dc voltage sensors. By using the proposed voltage balancing technique, the CHB converters do not need complicated dc link voltage controllers. As a result, the cost and complexity of the grid-tied converters can be significantly reduced. Simulations and experiments were conducted on a 7-level grid-tied CHB converter to validate the proposed voltage balancing technique with ASHCM-PWM modulation technique.**

***Index Terms*—Grid-tied cascaded H-bridge (CHB) converter, passive filter, selective harmonic current mitigation (SHCM)-pulse width modulation (PWM), sensor-less voltage balancing technique.**

I. Introduction

THE cascaded H-bridge (CHB) multilevel topology plays an important role in medium- and high-power electronics applications due to its low switching frequency, small filter size, low harmonics, low total harmonic distortion, and low electromagnetic interference [1], [2]. The CHB multilevel topology with isolated dc loads is used in many applications such as hybrid CHB multilevel inverter motor drive [3], CHB converter based solid-state transformer [4], CHB STATCOM [5], and CHB electrical vehicle charging station [6]. For these applications, the dc link voltage sensors, which are costly, are necessary to balance the dc link voltages of each H-bridge cell. Removing dc link voltage sensors and balancing the dc link voltages can significantly reduce the cost and increase reliability of the system.

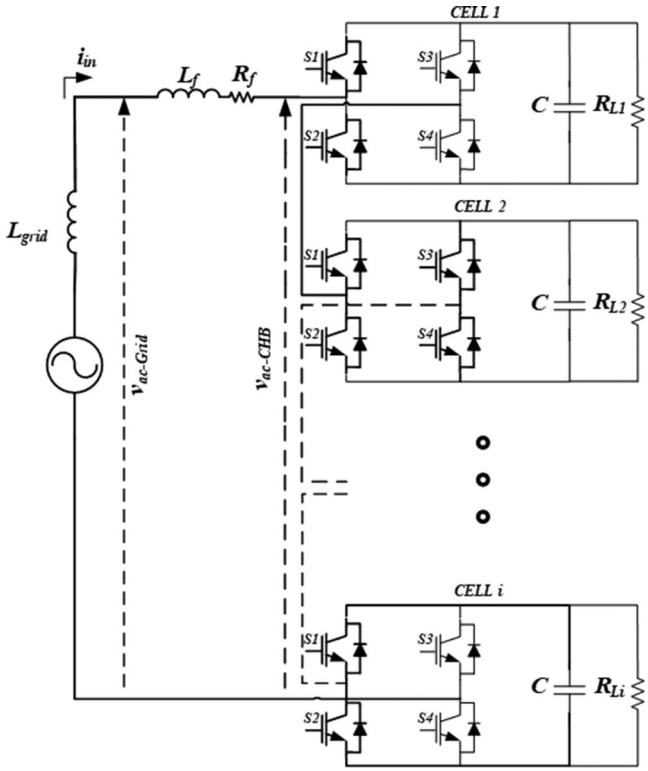

Fig. 1. Configuration of an *i*-cell, $(2i+1)$-level single-phase grid-tied CHB converter.

Fig. 1 shows a grid-tied, *i*-cell CHB ac/dc rectifier that has $2i+1$ output voltage levels [6]. The grid voltage is $v_{ac-\mathrm{Grid}}$. The dc link voltages are equal to V_{dc}. The input voltage of CHB is $v_{\mathrm{ac-CHB}}$, which is equal to the sum of the input voltages of all H-bridge cells. The current i_{in} flows from the power grid to CHB through two inductances, line inductance L_{grid}, and the inductance L_f of the coupling (filtering) inductor. The total inductance between the grid voltage source $v_{\mathrm{ac-Grid}}$ and the CHB rectifier is $L = L_{\mathrm{grid}} + L_f$. The dc links of the CHB ac/dc converter can be connected to any loads. For example,

Manuscript received January 22, 2017; revised June 3, 2017 and August 28, 2017; accepted October 19, 2017. Date of publication November 6, 2017; date of current version June 22, 2018. This work was supported by the National Science Foundation under Award Number 1540118. Recommended for publication by Associate Editor Georgios Konstantinou. *(Corresponding Author: Shuo Wang.)*

The authors are with the Department of Electrical and Computer Engineering, University of Florida, Gainesville, FL 32611 USA (e-mail: ahm1367@ufl.edu; shuowang@ieee.org).

Color versions of one or more of the figures in this paper are available online at http://ieeexplore.ieee.org.

Digital Object Identifier 10.1109/TPEL.2017.2770141

they could be connected to isolated dc/dc converters used to charge energy storage [6]. Therefore, they can be modeled as an identical load resistance $R_{L1} = R_{L2} = \cdots = R_{Li}$. In unequal dc load condition, R_{L1}, $R_{L2}, \ldots, R_{Li}$ (which are not equal to each other) can be connected to the dc link of each cell.

The main objectives of a grid-tied CHB converter in Fig. 1 are [7], [8]: 1) meet the current limits of power quality standards even there are grid voltage harmonics, which introduce current harmonics in $i_{\rm in}$, 2) control the injected active and reactive power to the power grid for the CHB converter, 3) regulate the dc link voltages of the CHB converter for all H-bridge cells, and 4) achieve high efficiency. The modulation technique, which is used for the grid-tied CHB converter, must achieve all the goals above [7], [8]. In actual applications, the modulation technique and a closed loop controller, which are used for the grid-tied CHB converter, should be able to achieve all the goals above [7], [8].

The modulation techniques of CHB converters can be categorized to two groups: 1) low frequency modulation techniques such as selective harmonic elimination-pulse width modulation (PWM) (SHE-PWM) [7], [9], [10], selective harmonic mitigation-PWM (SHM-PWM) [11]–[13], and selective harmonic current mitigation-PWM SHCM-PWM) [8]; 2) high frequency modulation techniques such as phase-shift PWM (PSPWM) [14], [15], and space vector modulation [16]. High frequency modulation techniques have high switching loss. As a result, the efficiency of CHB converter can be significantly reduced [2]. Therefore, it is promising to use low frequency modulation techniques for grid-tied CHB converters [2].

The low frequency SHE-PWM technique for a grid-tied CHB converter has been proposed in [17]. Even though this technique can eliminate the low-order injected current harmonics and regulate the dc link voltages of the CHB, the number of current/voltage harmonics, which can be eliminated, is very low [8]. So, for high-order noneliminated harmonics, an expensive and bulky passive filter must be used.

The SHM-PWM technique has been introduced in [11]. The voltage harmonics can meet the limits of voltage standards in dc/ac CHB inverters. However, this technique may not meet the current harmonic standards, such as IEEE-519 [18], even for low-order current harmonics [8].

To meet the current harmonic limits of power quality standards in full harmonic spectrum, SHCM-PWM technique has been introduced in [8]. In addition, the effects of grid voltage harmonics on current harmonics are considered in the designing of optimization and coupling inductance. However, the dc link voltage regulation was not investigated in [8] and [19]. The dc link voltage balancing technique for CHB converters with low-frequency SHE-PWM has been proposed in [17] and [20]. However, some switching transitions are used to balance dc link voltage; as a result, the number of switching transitions that can be used to eliminate current harmonics is reduced. This leads to lower number of harmonics that can be eliminated. In [7], a new voltage balancing technique by using the redundant states of CHB converters to generate different voltage levels has been proposed. By using the technique in [7], the number of switching transitions used to eliminate low-order harmonics is not reduced. However, i number of dc voltage sensors and a complex control algorithm must be used to balance the dc link voltages of the grid-tied i-cell CHB converter. This increases the cost and complexity of the grid-tied CHB converter.

In [21], a voltage balancing technique was proposed based on the modeling of unequal dc link voltages of STATCOM. Although the proposed technique can control the unequal dc link loads, it needs dc voltage sensors. In addition, the proposed technique is not suitable for active rectifier because the dc resistance must be estimated for different loads.

A phase shift SHE-PWM technique for the five-level H-bridge neutral-point-clamped (5L HNPC) topology have been introduced in [22] to calculate the solutions of SHE-PWM technique in wider modulation index range and balance the dc link voltages of 5L HNPC converters. Even though this technique can find the solutions of SHE-PWM technique in wide range and balance the dc link voltages, it needs dc link voltage sensor for each dc bus and one current sensor for input to predict the currents that flow through all capacitors. As a result, the cost of converter is increased but the reliability is reduced.

The symmetric SHCM-PWM technique was proposed in [8]. In this technique, instead of only eliminating the low-order voltage harmonics of CHB converters as used in SHE-PWM or only mitigating the low-order voltage harmonics of CHB converters as used in SHM-PWM, the current harmonics of grid-tied converters are mitigated to meet the current harmonic requirements of IEEE 519. The objective of SHCM-PWM technique is not the same as SHE-PWM and SHM-PWM even though voltage of CHB is controlled. In another words, in SHE-PWM and SHM-PWM techniques, the objective is to control the CHB voltage harmonics, but the current harmonics of grid-tied converters are not guaranteed to meet current harmonic standards. However, in the proposed SHCM-PWM technique, the objective is to control the current harmonics by controlling CHB voltages to meet current harmonic requirements which are critical requirements for grid-tied converters.

The asymmetric selective harmonic elimination (ASHE) technique for the CHB converter has been discussed in [23], [24]. The main advantages of ASHE-PWM are that it can control both the magnitudes and phases of the voltage harmonics of the CHB converter. On the other hand, for conventional SHE-PWM, only the magnitudes, but not the phases, of the CHB voltage harmonics can be controlled. The ASHE-PWM can also improve the solution range of the CHB converter [24].

In this paper, a dc link voltage balancing technique is proposed with an asymmetric SHCM-PWM (ASHCM-PWM) technique. The advantages of the ASHCM-PWM technique over conventional SHCM-PWM techniques [8] to control active power flowing through the grid-tied CHB converter are first discussed. Second, a dc link voltage balancing technique is proposed based on ASHCM-PWM to remove any dc link voltage sensors. The proposed technique can regulate the dc link voltages of grid-tied CHB converters for equal and unequal dc loads without reducing the number of switching transitions used for current harmonic mitigation. The proposed voltage balancing technique can also meet the current harmonic limits of the IEEE-519 standard. The

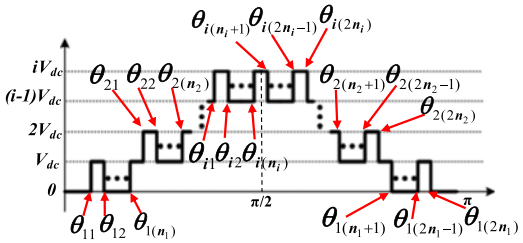

Fig. 2. Voltage waveform of a CHB converter using SHCM-PWM.

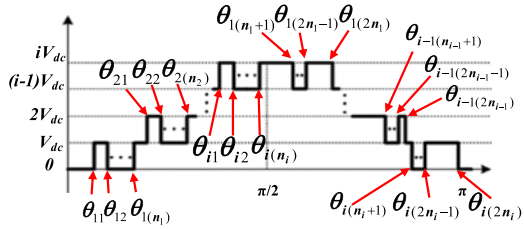

Fig. 3. Voltage waveform of a CHB converter using ASHCM-PWM.

proposed technique can be simply implemented for three-phase grid-tied converters. Because the proposed voltage balancing technique calculates the average power of each cell and based on it to regulate the dc link voltages for CHB cells, the complexity and cost of controller and sensors are significantly reduced. In addition, the reliability of grid-tied converters is improved because no dc link voltage sensors are used to balance the dc link voltages.

II. ASHCM-PWM Technique

Both conventional SHCM-PWM and the proposed ASHCM-PWM techniques use Fourier series to obtain voltage harmonics of $v_{\mathrm{ac-CHB}}$. The voltages and currents on the ac side of the single-phase CHB active rectifier in Fig. 1, when the parasitic resistance *R* of inductor *L* is ignored, can be written as

$$V_{\mathrm{ac-Grid-1}}\angle\theta_{\mathrm{Grid}} = j\omega L I_{\mathrm{in-1}}\angle\theta_{\mathrm{in}} + V_{\mathrm{ac-CHB-1}}\angle\theta_{\mathrm{CHB}} \tag{1}$$

$$V_{\mathrm{ac-Grid-}h}\angle\theta_{\mathrm{Grid-}h} = j\omega h L I_{\mathrm{in-}h}\angle\theta_{\mathrm{in-}h} + V_{\mathrm{ac-CHB-}h}\angle\theta_{\mathrm{CHB-}h}, h = 3, 5\ldots, \tag{2}$$

$$|I_{\mathrm{in-}h}| = \left|\frac{V_{\mathrm{ac-Grid-}h}\angle\theta_{\mathrm{Grid-}h} - V_{\mathrm{ac-CHB-}h}\angle\theta_{\mathrm{CHB-}h}}{\omega h L}\right| \tag{3}$$

where $V_{\mathrm{ac-Grid-1}}$, $V_{\mathrm{ac-CHB-1}}$, and $I_{\mathrm{in-1}}$ are the fundamental frequency grid voltage, CHB voltage, and the injected current of the CHB active rectifier, respectively. θ_{CHB}, θ_{Grid}, and θ_{in} are the fundamental frequency phases of CHB voltage, grid voltage, and injected current, respectively. In this paper, the phase of grid voltage is taken as the reference. Therefore, θ_{Grid} is always zero. When $h > 1$, $V_{\mathrm{ac-Grid-}h}$, $V_{\mathrm{ac-CHB-}h}$, and $I_{\mathrm{in-}h}$ are the grid voltage harmonics, CHB voltage harmonics, and injected current harmonics, respectively. $\theta_{\mathrm{CHB-h}}$, $\theta_{\mathrm{Grid-}h}$, and $\theta_{\mathrm{in-}h}$ are the phases of CHB voltage, grid voltage, and injected current, respectively, for the *h*th-order harmonic.

For the half-period $v_{\mathrm{ac-CHB}}$ waveform in Figs. 2 and 3, the number of switching transitions in a half-period of the *k*th cell is $2n_k$, $k = 1, 2, \ldots, i$. Moreover, the total number of switching transitions in a half-period is equal to $K = 2(n_1 + n_2 + n_3 + \ldots + n_i)$. The waveform in Fig. 2 is odd quarter wave symmetry, so its Fourier series equations are

$$v_{\mathrm{ac-CHB}}(t) = \sum_{h=1}^{\infty}\frac{4V_{dc}}{\pi h}\left(b_h \sin\left(h\omega t + h\theta_{\mathrm{CHB}}\right)\right)$$
$$b_h = \left(\cos\left(h\theta_{11}\right) - \cos\left(h\theta_{12}\right) + \ldots. + \cos\left(h\theta_{i(n_i)}\right)\right). \tag{4}$$

In (4), because the waveform is odd quarter wave symmetry, the even-order harmonics of b_h are zero. The constraints of switching angles is [8]

$$0 < \theta_{11} < \theta_{12} < \ldots. < \theta_{i(n_i)} < \frac{\pi}{2}. \tag{5}$$

As will be discussed in the next section, to balance the dc link voltages of the CHB converter, the average power of all cells must be controlled because the loads of cells can be equal or unequal. In Fig. 2, because the switching order in the first-quarter period is cell_1, cell_2, …, celli, the switching order in the second-quarter period is cell_i, cell_{i-1}, …, cell1, and the two switching angles of each cell are symmetric to phase $\pi/2$, when there is active power flowing through the CHB converter and the dc link voltages of all cells are V_{dc}, with the constraints of (5), the following condition holds for the CHB converter

$$\begin{cases} P_{\mathrm{avg-Cell-1}} \geq P_{\mathrm{avg-Cell-2}} \geq \cdots \geq P_{\mathrm{avg-Cell-}i}, \\ \quad \text{when} -\dfrac{\pi}{2} \leq (\theta_{\mathrm{Grid}} - \theta_{\mathrm{in}}) \leq \dfrac{\pi}{2} \\ P_{\mathrm{avg-Cell-1}} \leq P_{\mathrm{avg-Cell-2}} \leq \cdots \leq P_{\mathrm{avg-Cell-}i}, \\ \quad \text{when} \dfrac{\pi}{2} \leq (\theta_{\mathrm{Grid}} - \theta_{\mathrm{in}}) \leq \dfrac{3\pi}{2} \end{cases} \tag{6}$$

where $P_{\mathrm{avg-Cell-}k}$ is the average power of *k*th cell of CHB converter. The equal relationship between the average powers of cells in (6) only happens when the switching angles of different cells in rising and falling switching transitions in each half-period are at the same time, which is unacceptable for multilevel converters. From (6), it is obvious that with the SHCM-PWM technique in Fig. 2, it is impossible to balance the dc link voltages of the CHB converter if there is active power flowing through the CHB converter for equal load condition or if the required active power of these cells does not meet (6) for unequal loads.

To solve this issue, ASHCM-PWM technique is introduced to balance the dc link voltages in this paper. The half-period waveform with ASHCM-PWM is shown in Fig. 3. The two switching angles of each cell are asymmetric to phase $\pi/2$. The

TABLE I
HARMONIC LIMITS OF IEEE 519 2014 STANDARD [18]

$I_{\rm sc}/I_L \le 20$	<11	$11 \le h < 17$	$17 \le h < 23$	$23 \le h < 35$	$35 \le h \le 50$	$C_{\rm TDD}$
$C_{h\ \&\ \rm TDD}$	4%	2%	1.5%	0.6%	0.3%	5%

Fourier series equations of ASHCM-PWM are

$$v_{\rm ac-CHB}(t) = \sum_{h=1}^{\infty}\left(\frac{2V_{\rm dc}}{\pi h}(a_h\ \cos(h\,\omega t + h\,\theta_{\rm CHB}) + b_h\ \sin(h\,\omega t + h\theta_{\rm CHB}))\right)$$

$$a_h = (-\sin(h\,\theta_{11}) + \sin(h\,\theta_{12}) - \cdots - \sin(h\,\theta_{i(2n_i)})))$$
$$b_h = (\cos(h\,\theta_{11}) - \cos(h\,\theta_{12}) + \cdots + \cos(h\,\theta_{i(2n_i)})) \quad (7)$$

where, in (7), because the waveform in Fig. 3 is half-wave symmetry, the a_h and b_h of the even-order harmonics are zero. $\theta_{{\rm CHB}-h}$ in (2) is the phase of the hth-order CHB voltage harmonic, $(2/\pi)b_1$ is defined as the modulation index M_a of the CHB converter

$$\theta_{{\rm CHB}-h} = h\theta_{\rm CHB} + \tan^{-1}\left(\frac{a_h}{b_h}\right). \quad (8)$$

The phase of fundamental harmonic in CHB converter is

$$\theta_{{\rm CHB}-1} = \theta_{\rm CHB} + \tan^{-1}\left(\frac{a_1}{b_1}\right). \quad (9)$$

The modulation index of $v_{\rm ac-CHB}(t)$ for ASHCM-PWM is

$$\frac{\pi}{2}M_a = b_1 = \left(\cos(\theta_{11}) - \cos(\theta_{12}) + \cdots - \cos\left(\theta_{i(2n_i)}\right)\right). \quad (10)$$

As shown in Fig. 3, because the switching order in the first-quarter period is $\rm cell_1$, cell2, …, celli, the switching order of the second-quarter period is $\rm cell_1$, cell2, …, celli, and the two switching angles of each cell are asymmetric to phase π/2, the active power can be equally or unequally injected to all cells by regulating switching angles. In addition, in order to help find solutions based on [24] using optimization technique, the following switching angle constraints are used for the proposed ASHCM-PWM technique

$$\begin{aligned}
&0 < \theta_{11} < \theta_{12} < \cdots < \theta_{1n_1} < \theta_{1(n_1+1)} < \cdots < \theta_{1(2n_1)} < \pi\\
&0 < \theta_{21} < \theta_{22} < \cdots < \theta_{2n_2} < \theta_{2(n_2+1)} < \cdots < \theta_{2(2n_2)} < \pi\\
&\cdots\\
&0 < \theta_{i1} < \theta_{i2} < \cdots < \theta_{{\rm in}_i} < \theta_{i(n_i+1)} < \cdots < \theta_{i(2n_i)} < \pi.
\end{aligned} \quad (11)$$

The proposed ASHCM-PWM technique can work similarly to SHCM-PWM in [8] to meet the current limits of the IEEE-519 with ease.

Table I shows the current harmonic limits of the IEEE 519 when $I_{\rm sc}/I_L \le 20$. $I_{\rm sc}$ is the short-circuit current of the grid-tied CHB converter at point of common coupling (PCC). I_L is the maximum demand load current. C_h is harmonic current limit and $C_{\rm TDD}$ is total demand distortion limit. In the proposed technique, the worst grid short-circuit $I_{\rm sc}/I_L$ scenario in the IEEE 519 2014 is considered. Because as long as the worst scenario is met, other scenarios can be met, it is unnecessary to consider all scenarios in the paper.

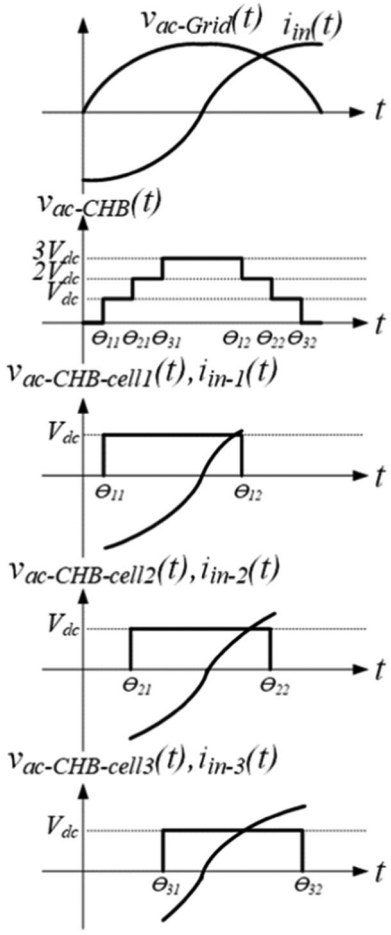

Fig. 4. Time domain waveforms of the $v_{\rm ac-CHB}(t)$, $i_{\rm in}(t)$, and $v_{\rm ac-Grid}(t)$ of a 3-cell CHB in a half-period.

III. PROPOSED VOLTAGE BALANCING TECHNIQUE FOR GRID-TIED CHB CONVERTERS

To balance the dc link voltages of the grid-tied CHB converter for equal or unequal dc loads in Fig. 1, the average power of each CHB cell must be controlled equally or unequally, respectively. The average power that flows through the cells is determined by the fundamental voltage and current flowing through the cells. Fig. 4 shows an example of the staircase waveform for a 3-cell CHB converter when each switch of the CHB converter turn ON and OFF only once in each half period. $v_{ac-CHB-cell1}(t)$, $v_{ac-CHB-cell2}(t)$, and $v_{ac-CHB-cell3}(t)$ are the ac CHB

voltages of three cells. $i_{\text{in}-1}(t)$, $i_{\text{in}-2}(t)$, and $i_{\text{in}-3}(t)$ are the currents of three cells.

The average power for the *k*th cell of the CHB converter can be derived as

$$P_{\text{avg}-\text{Cell}-k} = \frac{1}{t_2 - t_1}\int_{t_1}^{t_2} (v_{\text{ac}-\text{CHB}-\text{cell}k}(t) i_{\text{in}}(t))dt \quad (12)$$

where the *k*th cell turns ON during $[t_1,\, t_2]$. $v_{\text{ac}-\text{CHB}-\text{cell}k}(t)$ in Fig. 3 is half-wave symmetry and it can be derived from (7) as

$$v_{\text{ac}-\text{CHB}-\text{cell}k}(t) = \sum_{h=1}^{\infty}\left(\frac{2V_{\text{dc}}}{\pi h}(a_h\, \cos(h\,\omega t + h\,\theta_{\text{CHB}}) + b_h\, \sin(h\,\omega t + h\,\theta_{\text{CHB}}))\right)$$

$$a_h = (-\sin(h\,\theta_{k1}) + \sin(h\,\theta_{k2}) - \cdots - \sin(h\theta_{k(2n_k)}))$$

$$b_h = (\cos(h\,\theta_{k1}) - \cos(h\,\theta_{k2}) + \cdots + \cos(h\,\theta_{k(2n_k)})). \quad (13)$$

Because only the fundamental current of the CHB converter generates power, only the fundamental sinusoidal $i_{\text{in}}(t)$ is considered in average power calculation

$$i_{\text{in}}(t) = \sqrt{2} I_{\text{in}}\, \sin\,(\omega t + \theta_{\text{in}}) \quad (14)$$

where ω is the fundamental frequency of grid voltage. The average power of cell 1 can be calculated from (12)–(14) and shown as

$$\begin{aligned} P_{\text{avg}-\text{Cell}-1} = {} & \frac{\sqrt{2}V_{\text{dc}} I_{\text{in}}}{\pi}((\cos(\theta_{11}) - \cos(\theta_{12}) \\ & + \cdots + \cos(\theta_{1(2n_1)}))\cos(\theta_{\text{in}} - \theta_{\text{CHB}}) \\ & - (-\sin(\theta_{11}) + \sin(\theta_{12}) - \cdots - \sin(\theta_{1(2n_1)})) \\ & \times \sin(\theta_{\text{in}} - \theta_{\text{CHB}})). \end{aligned} \quad (15)$$

The average power of other cells can similarly be calculated. As shown in (15), the average power depends on switching angles, θ_{CHB} and θ_{in}. The balancing condition for equal loads is

$$P_{\text{avg}-\text{Cell}-1} = P_{\text{avg}-\text{Cell}-2} = P_{\text{avg}-\text{Cell}-3} = \cdots = P_{\text{avg}-\text{Cell}-i}. \quad (16)$$

In general, when the ratios between the average powers of each cell of the CHB converter are

$$\frac{P_{\text{avg}-\text{Cell}-1}}{P_{\text{avg}-\text{Cell}-2}} = g_1, \frac{P_{\text{avg}-\text{Cell}-1}}{P_{\text{avg}-\text{Cell}-3}} = g_2, \ldots, \frac{P_{\text{avg}-\text{Cell}-1}}{P_{\text{avg}-\text{Cell}-i}} = g_{i-1} \quad (17)$$

the balancing condition for equal and unequal loads can be derived as

$$\begin{aligned} P_{\text{avg}-\text{Cell}-1} &= g_1 P_{\text{avg}-\text{Cell}-2} = g_2 P_{\text{avg}-\text{Cell}-3} = \cdots \\ &= g_{i-1} P_{\text{avg}-\text{Cell}-i}. \end{aligned} \quad (18)$$

Switching angles can be solved from (16) and (18) for different θ_{CHB} and θ_{in}. The θ_{CHB} can be obtained based on θ_{in}, from Fig. 1 as

$$\theta_{\text{CHB}} = \text{Arg}\left(\frac{\sqrt{2}V_{\text{ac}-\text{Grid}}\angle 0 - (R + j\omega L)\sqrt{2} I_{\text{in}}\angle\theta_{\text{in}}}{4V_{\text{dc}}/\pi}\right). \quad (19)$$

Moreover, the switching angles of the converter are also determined by the modulation index. The modulation index of the CHB converter as a function of I_{in} and θ_{in} is

$$M_a = \left|\frac{\sqrt{2}V_{\text{ac}-\text{Grid}}\angle 0 - (R + j\omega L)\sqrt{2} I_{\text{in}}\angle\theta_{\text{in}}}{4V_{\text{dc}}/\pi}\right|. \quad (20)$$

Switching angles can be solved from (15) to (20) for different modulation indices and θ_{CHB}. On the other hand, because the dc link voltages of the CHB converter are equal, the active (average) power of the CHB converter for equal or unequal loads is, if the switching power loss is ignored

$$\sum_{k=1}^{i} P_{\text{avg}-\text{Cell}-k} = \sum_{k=1}^{i}\frac{kV_{\text{dc}}^2}{R_{lk}} = V_{\text{ac}-\text{Grid}} I_{\text{in}}\, \cos(-\theta_{\text{in}}) - RI_{\text{in}}^2. \quad (21)$$

For different loads and current phase θ_{in}, the root mean square (RMS) current I_{in} can be derived from (21). Equation (21) has solutions when θ_{in} meets the following condition:

$$\begin{aligned} -\arccos\left(\left|\sqrt{\frac{4R\sum_{k=1}^{i} P_{\text{avg}-\text{Cell}-k}}{(V_{\text{ac}-\text{Grid}})^2}}\right|\right) < \theta_{\text{in}} \\ < \arccos\left(\left|\sqrt{\frac{4R\sum_{k=1}^{i} P_{\text{avg}-\text{Cell}-k}}{(V_{\text{ac}-\text{Grid}})^2}}\right|\right). \end{aligned} \quad (22)$$

θ_{in} in (22) determines the injected or absorbed active or reactive power to or from the power grid. θ_{in} depends on the parameters of the converter, load, and the voltage of the grid.

The left side of (21) is average power dissipated by all of the dc loads. If the converter also controls the reactive power injected to the power grid [19], the following equations hold:

$$\begin{aligned} P_{\text{avg}-\text{CHB}-\text{dc}}{}^* &= V_{\text{ac}-\text{Grid}} I_{\text{in}}\, \cos\,(-\theta_{\text{in}}) - RI_{\text{in}}^2 \\ Q_{\text{CHB}-\text{ac}}{}^* &= V_{\text{ac}-\text{Grid}} I_{\text{in}}\, \sin\,(-\theta_{\text{in}}) \end{aligned} \quad (23)$$

where $P_{\text{avg}-\text{CHB}-\text{dc}}{}^*$ and $Q_{\text{CHB}-\text{ac}}{}^*$ are the references of active power dissipated by dc loads and the reactive power injected to ac power grid, respectively.

IV. Solving Switching Angles for Voltage Balancing Technique With ASHCM-PWM

For the proposed ASHCM-PWM, the critical parameters such as the lowest number of switching transitions, the lowest coupling inductance, and the highest order of harmonics that should be mitigated must be designed. Based on (15)–(18) and the equations of SHCM-PWM in [8], the equation set (24) can be derived for ASHCM-PWM technique to meet the current harmonic and TDD limits of the IEEE-519, when the dc link voltages of converter are balanced based on (15)–(18) for equal or unequal

TABLE II
CIRCUIT PARAMETERS

Parameter	Symbol	Value
Line frequency	F	60 Hz
AC grid voltage (RMS)	$V_{\mathrm{ac-Grid}}$	110 V
Total rated power	S_{total}	1.550 kVA
Maximum demand load (RMS)	I_L	14.14 A
Number of H-bridge cells	I	3
Dc link voltage	V_{dc}	70 V
Number of switching transitions	K	18
Highest order of mitigated harmonic	H	49th
Resistance of inductance	R	0.0643 pu
Impedance of dc link capacitor	$1/\omega C$	0.0775 pu

TABLE III
REQUIRED REACTANCE (PU) TO MEET CURRENT HARMONICS OF THE IEEE-519 2014 FOR DIFFERENT GRID VOLTAGE HARMONICS

Grid Voltage Harmonics	Required Reactance for Coupling Inductor (pu)	The Number of Low-Order Harmonics and TDD That are Controlled
Meet the worst scenario of IEEE-519	0.63	50 with TDD
Grid voltage harmonics in Figs. 12 and 13	0.34	50 with TDD
Ideal (No voltage harmonics)	0.24	50 with TDD
Ideal (No voltage harmonics)	0.1	20 without TDD

loads

$$\begin{cases} \left(\cos\theta_{11} - \cos\theta_{12} + \cos\theta_{13} + \cdots - \cos\theta_{i(2n_i)}\right) = \dfrac{\pi}{2} M_a \\ \left(-\sin\theta_{11} + \sin\theta_{12} - \sin\theta_{13} - \cdots + \sin\theta_{i(2n_i)}\right) = 0 \\ I_{\mathrm{in}-h} \le \dfrac{|V_{\mathrm{ac-Grid}-h}| + |V_{\mathrm{ac-CHB}-h}|}{|\omega h L I_L|} \le C_h, \quad h = 3, 5, 7, \ldots, \\ \sqrt{\left(\dfrac{I_{\mathrm{in}-3}}{I_L}\right)^2 + \left(\dfrac{I_{\mathrm{in}-5}}{I_L}\right)^2 + \cdots + \left(\dfrac{I_{\mathrm{in}-h}}{I_L}\right)^2 + \cdots} \le C_{\mathrm{TDD}} \\ P_{\mathrm{avg-Cell}-1} = g_1 P_{\mathrm{avg-Cell}-2} = \cdots = g_{i-1} P_{\mathrm{avg-Cell}-i} \end{cases} \tag{24}$$

where, in (24), the first two equations control the magnitude of fundamental CHB voltage. To control the phase of CHB converter in ASHCM-PWM, there are two techniques: 1) control a_1 and b_1 in (7) to obtain the desired CHB voltage and phase and do not make any phase shift on the ωt, which is the angle of the grid voltage, 2) eliminate the a_1 as shown in (24) and solve (24) for different M_a. Then, the phase shift θ_{CHB} will be added to ωt. In this paper, the second approach is used to control magnitude and phase of the CHB with a_1 equal to zero. The third equation in (24) guarantees $I_{\mathrm{in}-h}$ is below the current harmonic limits. The fourth equation in (24) guarantees i_{in} is within the TDD limit. The $I_{\mathrm{in}-h}$ in the third and fourth equations of (24) are calculated based on the worst scenario of (3) when the CHB voltage and the grid voltage harmonics are out of phase. In other words, $I_{\mathrm{in}-h}$ is the highest when the phase difference between $v_{\mathrm{ac-CHB}-h}(\mathrm{t})$ and $v_{\mathrm{ac-Grid}-h}(\mathrm{t})$ is 180°, so the absolute values of $V_{\mathrm{ac-CHB}-h}$ and $V_{\mathrm{ac-Grid}-h}$ are added up in (24). The fifth equation in (24) balances the dc link voltages of the CHB converter based on (17) and (18). It is worth noting that the ranges of grid voltage and load are needed for the proposed technique to meet (24).

The parameter design guidelines for the SHCM-PWM technique have been discussed in [8]. These guidelines can also be applied to ASHCM-PWM technique. Table II gives the designed parameters of the CHB converter with ASHCM-PWM technique. In this paper, the dc link voltage of CHB converter is 70 V. The range of θ_{in} can be calculated based on (22) for the designed parameters in Table II. The required inductances in pu for the grid-tied CHB converter for the different grid voltage harmonics are shown in Table III. To find these inductances, the algorithm in [8] is used to design the parameters for ASHCM-PWM technique. As shown in the first row of Table III, for the worst scenario, the inductance was designed to meet current harmonic limits when the grid voltage distortion, which is as high as the voltage harmonic requirements of the IEEE 519, also causes the current harmonics. The required minimum inductance is calculated as 0.63 pu to meet the limits of all harmonics with the worst grid voltage harmonics defined in the IEEE-519. However, when the grid voltage harmonics are ignored (ideal grid voltage), only the minimum 0.24 pu inductance is required to meet both harmonics up to the 50th and TDD limits. Moreover, only the minimum 0.1 pu is required to meet current harmonic limits up to the 20th without meeting the TDD limit. In this paper, to design the inductance to meet the current harmonic limit with actual grid voltage harmonics, which can be extracted from FFT in Fig. 12(a), the minimum 0.34 pu inductance is required based on [8]. All of the simulation and experimental results are based on this. From Table III, it can be concluded that smaller inductance can only control smaller number of current harmonics. In order to meet all of the current harmonics, enough inductance must be needed. In literatures, small inductance is used with ideal grid voltage, but the inductance cannot meet all of the current harmonics under the conditions defined in Table III. It is worth noting that if the inductance is smaller than the values in the Table III, i_{in} cannot meet the current harmonic requirements in the corresponding scenario. If the RMS of CHB current I_{in} changes from 0 to I_L (14.14 A), the total average power of the loads are from 1 to 1550 W and the phase of current θ_{in} is limited by (22), the modulation index M_a of the CHB voltage can be derived in Fig. 5 based on (20), (21), and the parameters in Table II with 0.34 pu inductance.

To solve the equations of ASHCM-PWM technique with the proposed voltage balancing technique, the least square error technique is first used to find initial values for the switching angles of the CHB converter. The heuristic multiobjective particle swarm optimization (MOPSO) technique [25] is used to find the solutions for the proposed technique in a wide modulation index range to meet all of the objectives in (24). Fig. 6 shows the subset of the Fig. 5, in which the switching angle solutions for the 3-cell CHB converter with the circuit parameters in Tables II and III when g_1 and g_2 are equal to 1, can be found with MOPSO. I_{in} is from 1 to 20 A and the current phase meets the limits of

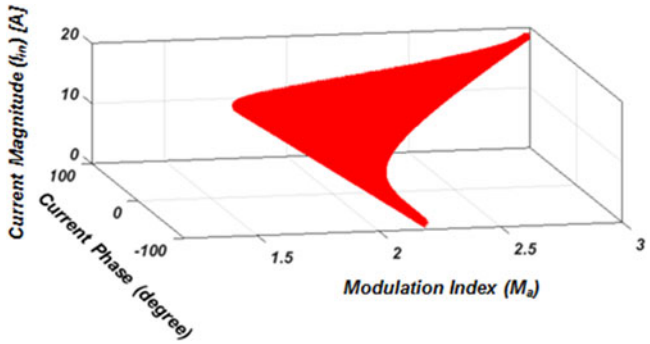

Fig. 5. Modulation index and phase of the fundamental CHB voltage based on (16)–(19).

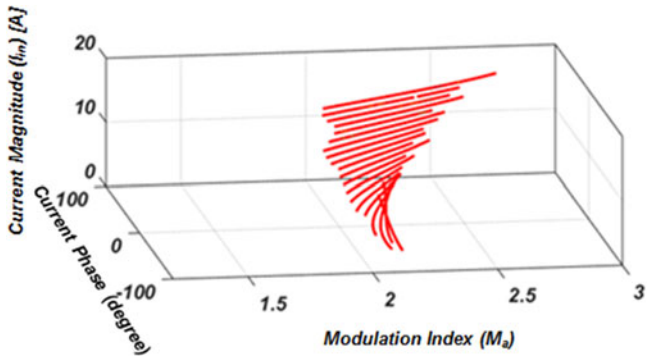

Fig. 6. Solutions of the proposed technique with the circuit parameters in Tables II and III.

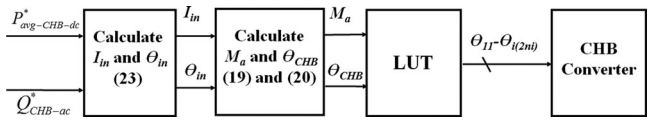

Fig. 7. Proposed sensor-less dc link voltage balancing technique.

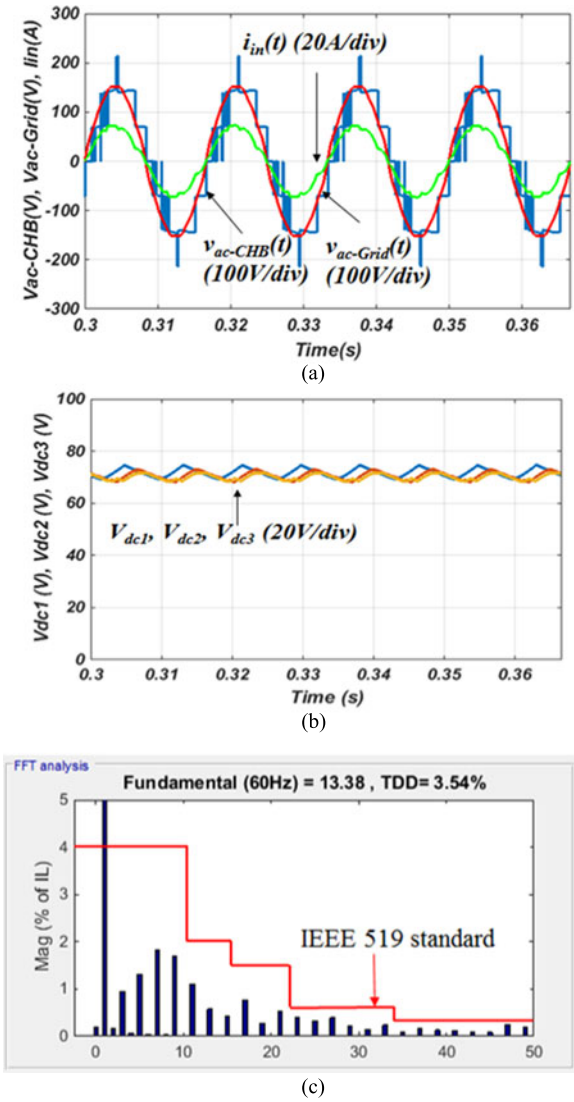

Fig. 8. Simulation result of the proposed sensor-less voltage balancing technique when $P_{\mathrm{avg-CHB-dc}}{}^* = 980$ W, and $V_{\mathrm{dc}} = 70$ V. (a) Time domain waveforms of $v_{\mathrm{ac-CHB}}(t)$, $v_{\mathrm{ac-Grid}}(t)$, and $i_{\mathrm{in}}(t)$. (b) Time domain waveforms of V_{dc1}, V_{dc2}, and V_{dc3}. (c) Current harmonic spectrum of $i_{\mathrm{in}}(t)$.

(22). If (24) has solutions in the range of Fig. 5, the converter can work in all range of the active and reactive power when grid voltage is 110 V. To clearly compare the range of obtained solutions in Fig. 6 with Fig. 5, only the modulation indices of the obtained switching angles are shown in Fig. 6. As shown in Fig. 6, the solutions were found for the proposed sensor-less voltage balancing technique in a wide range of Fig. 5. To consider the disturbances of the grid voltage or load, the (15)–(24) can be solved offline similar to Fig. 6 for different grid voltage and load conditions. The obtained solutions give the operation range of the converter.

Fig. 7 shows the block diagram of implementing the proposed technique without using any sensors for dc link voltage balancing. $P_{\mathrm{avg-CHB-dc}}{}^*$ and $Q_{\mathrm{CHB-ac}}{}^*$ are the references of controller for the grid-tied converter.

An open-loop controller is used in Fig. 7 to demonstrate the principle of the proposed technique. In actual applications, a closed loop controller, which can sense grid voltage and grid current, can be used to control $P_{\mathrm{avg-CHB-dc}}{}^*$ and $Q_{\mathrm{CHB-ac}}{}^*$ references to achieve dc link voltage balance. The current magnitude I_{in} and phase θ_{in} can be calculated from (23). From (19) and (20), the modulation index M_a and CHB voltage phase θ_{CHB} can be calculated. Finally, the switching angles of the CHB converter are solved from equation set (24) with MOPSO. The solved switching angles are applied to the converter. It does not, therefore, need to consider the actual load resistances to balance the dc link voltages.

V. Simulation and Experimental Results

To validate the proposed sensor-less dc link voltage balancing technique with ASHCM-PWM, the simulations and experiments were conducted on a 7-level CHB converter. MATLAB Simulink was used for the simulation. The main objectives of the simulations and experiments are: 1) balance the dc link voltages to 70 V, 2) meet the current harmonic and TDD limits of IEEE-519, 3) keep the fundamental of $i_{\mathrm{in-1}}(t)$ in phase with $v_{\mathrm{ac-Grid-1}}(t)$ and control its magnitude, and 4) investigate

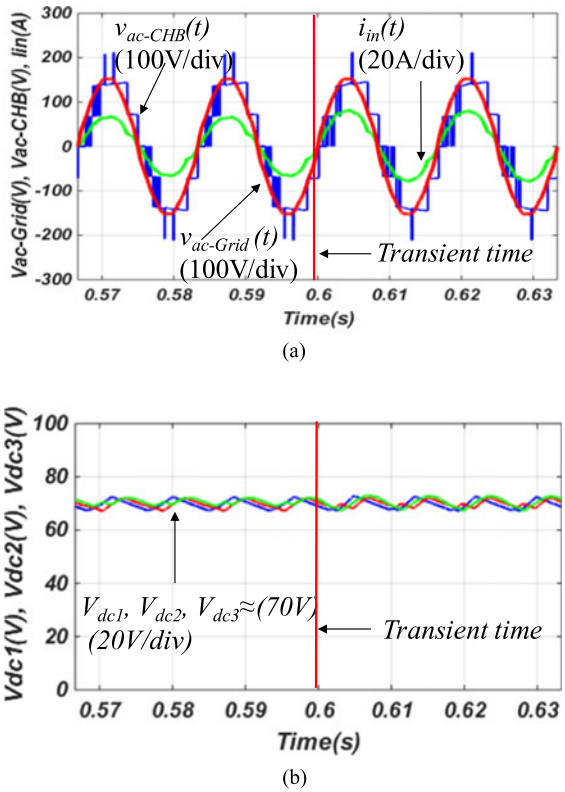

Fig. 9. Simulation result of the proposed sensor-less voltage balancing technique in transient condition when the active power of cell 3 is changed from 326.67 (equal loads) to 515.25 W (unequal loads), and $V_{\rm dc} = 70$ V. (a) Time domain waveforms of $v_{\rm ac-CHB}(t)$, $v_{\rm ac-Grid}(t)$, and $i_{\rm in}(t)$. (b) Time domain waveforms of V_{dc1}, V_{dc2}, and V_{dc3}.

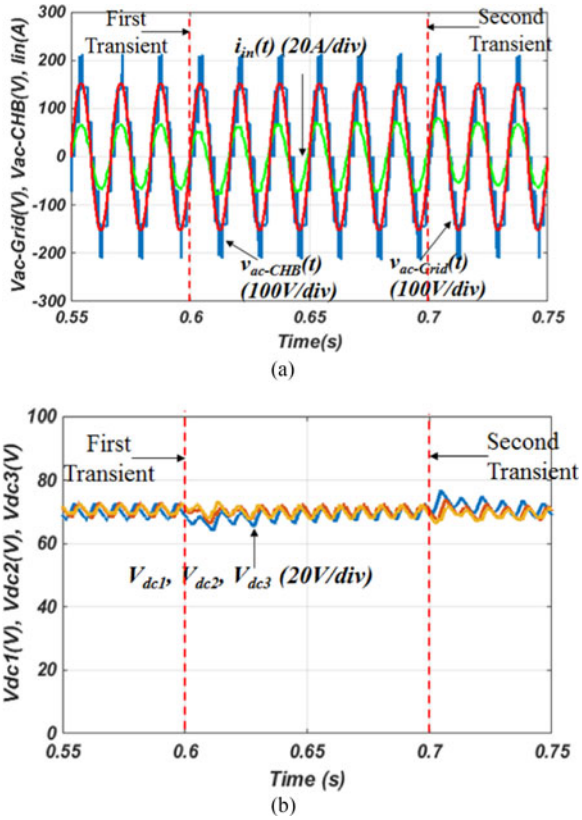

Fig. 10. Simulation result of the proposed sensor-less voltage balancing technique in dynamic condition when the active and reactive power at PCC is changed from 1030 to 1030 W–375 VAr at $t = 0.6$ s and retuned to 1030 W at $t = 0.7$ s. (a) Time domain waveforms of $v_{\rm ac-CHB}(t)$, $v_{\rm ac-Grid}(t)$, and $i_{\rm in}(t)$. (b) Time domain waveforms of V_{dc1}, V_{dc2}, and V_{dc3}.

using the proposed technique to balance the dc link voltages with unequal loads.

In the first simulation, the active power flowing through all of the dc loads are 980 W. No reactive power is injected or absorbed from the power grid. Fig. 8 shows the $v_{\rm ac-CHB}(t)$, $v_{\rm ac-Grid}(t)$, and $i_{\rm in}(t)$ for the proposed voltage balancing technique with ASHCM-PWM technique. Fig. 8(a) shows the time domain waveforms. The modulation index of converter is 2.165. The fundamental of $i_{\rm in}(t)$ is in phase with $v_{\rm ac-Grid}(t)$. In Fig. 8(b), the average dc link voltages of the three cells are regulated to 70 V. The second-order harmonic due to instantaneous power is observed in the voltage waveforms. In Fig. 8(c), the current harmonics of the CHB converter meet the limits of the IEEE-519 [18] up to the 50th-order harmonic. TDD is 3.54%, which meets the 5% limit of the IEEE-519. The dc link voltage ripple in Fig. 8(b) is due to the second-order harmonic of instantaneous power that is generated on the ac side of converter. Because in the proposed technique, the average power instead of instantaneous power of CHB is used as the reference power of each cell, the second-order harmonic is not shown in (15) because the average of the second-order harmonic power is zero in one period. In the second simulation, the active power flowing through all of the dc loads are 980 W before $t = 0.6$ s. Each cell has around 326.7 W. No reactive power is injected or absorbed from the power grid. At $t = 0.6$ s, the load of the third cell is increased by 57% from 326.67 to 515.25 W. The modulation index of the converter is changed from 2.152 to 2.180 correspondingly. Fig. 9 shows the $v_{\rm ac-CHB}(t)$, $v_{\rm ac-Grid}(t)$, and $i_{\rm in}(t)$ for the proposed voltage balancing technique with ASHCM-PWM technique with equal ($t < 0.6$ s) and unequal ($t > 0.6$ s) loads. Fig. 9(a) shows the time domain waveforms. $i_{\rm in}(t)$ is in phase with $v_{\rm ac-Grid}(t)$. In Fig. 9(b), the dc link voltages of three cells are regulated to 70 V.

In the last simulation in Fig. 10, the dynamic performance of the proposed voltage balancing technique is simulated with equal dc link loads. The active and reactive power, which is injected from the power grid to the converter, is changed from 1030 W to 1030 W–375 VAr at $t = 0.6$ s. The power of rectifier returns to 1030 W at $t = 0.7$ s. Fig. 10(a) shows the time domain waveform of the proposed technique for $v_{\rm ac-CHB}(t)$, $v_{\rm ac-Grid}(t)$, and $i_{\rm in}(t)$. As discussed in [19] and shown in Fig. 10(a), ASHCM-PWM has a weak dynamic performance, so it generates a small dc term when the active and reactive power is changed. This is actually true for all low frequency modulation techniques. This can be solved by applying high-frequency PSPWM during the dynamic period [19]. The modulation index of converter is changed between 2.165 and 2.347 during the first transient condition. In Fig. 10(b), the dc link voltages of the three cells are regulated to be around 70 V within dynamic period. Table IV shows the switching angles sets of these three

TABLE IV
SWITCHING ANGLE SETS (DEGREE) FOR SIMULATIONS AND EXPERIMENTS WITH THE PROPOSED TECHNIQUE

Switching Angles	First Case	Second Case (Before Transient)	Second Case (After Transient)	Third Case (Before Transient)	Third Case (After Transient)
θ_{11}	41	18	0	41	13
θ_{12}	45	23	1	45	23
θ_{13}	54	26	15	54	32
θ_{21}	10	10	10	10	26
θ_{22}	12	16	12	12	34
θ_{23}	46	31	33	46	41
θ_{31}	0	41	14	0	9
θ_{32}	1	49	15	1	11
θ_{33}	5	53	27	5	47
θ_{14}	67	43	25	67	56
θ_{15}	87	45	40	87	67
θ_{16}	169	95	89	169	98
θ_{24}	51	35	49	51	69
θ_{25}	67	67	86	67	87
θ_{26}	134	135	135	134	168
θ_{34}	7	68	33	7	47
θ_{35}	16	93	52	16	57
θ_{36}	90	167	168	90	140

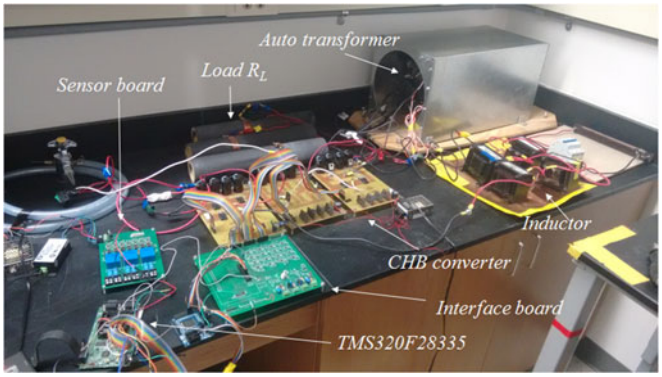

Fig. 11. Hardware prototype of a 7-level grid-tied CHB converter.

simulations results. The same switching angle sets are also used in the experiments in this paper.

For the experimental results, the 3-cell 7-level CHB converter was connected to the power grid with the same parameters shown in Table II when 0.34 pu coupling inductance is used. The TMS320F28335 microprocessor is used to generate the switching angles for the proposed technique. The hardware prototype of the grid-tied CHB converter is shown in Fig. 11.

In the first experiment, the dc link voltages of the CHB converter are equal to 70 V. Fig. 12 shows the $v_{\mathrm{ac-CHB}}(t)$, $v_{\mathrm{ac-Grid}}(t)$, and $i_{\mathrm{in}}(t)$ for the proposed voltage balancing technique with ASHCM-PWM modulation technique. As shown in Fig. 12(a), $i_{\mathrm{in}}(t)$ and $v_{\mathrm{ac-Grid}}(t)$ are in phase. The modulation index of the converter is 2.165. Fig. 12(b) shows the dc link voltages of the CHB converter with the proposed voltage balancing technique. As shown in Fig. 12(b), all of the dc link voltages are regulated to be around 70 V. Fig. 12(c) shows the current harmonic spectrums of I_{in} with the proposed technique. It is obvious that all current harmonics and TDD can meet the limits of the IEEE-519 standard [18] when the grid voltage has low-order voltage harmonics as shown in Fig. 12(a). The even-order

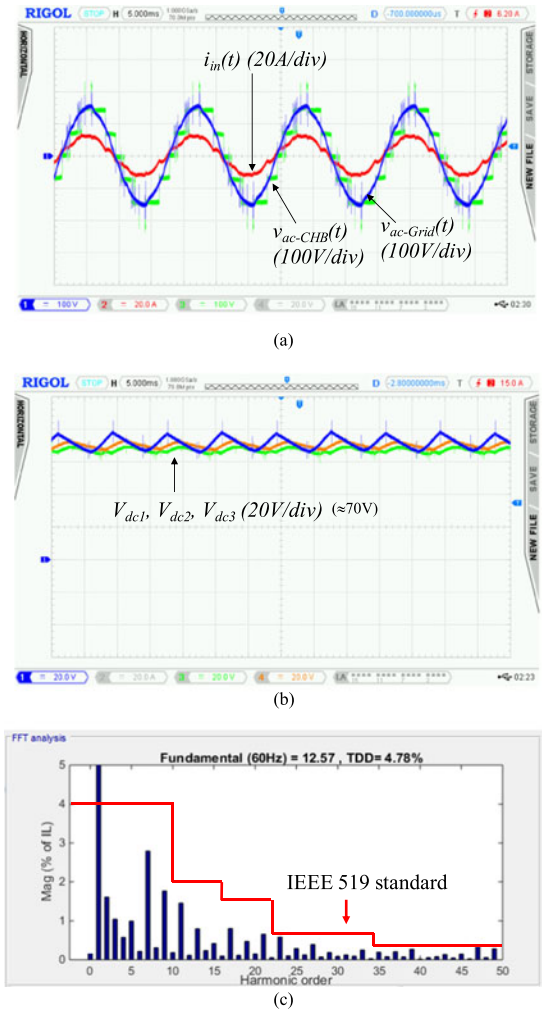

Fig. 12. Experimental result of the proposed sensor-less voltage balancing technique when $P^{*}_{\mathrm{avg-CHB-dc}} = 980$ W, and $V_{\mathrm{dc}} = 70$ V. (a) Time domain waveforms of $v_{\mathrm{ac-CHB}}(t)$, $v_{\mathrm{ac-Grid}}(t)$, and $i_{\mathrm{in}}(t)$. (b) Time domain waveforms of V_{dc1}, V_{dc2}, and V_{dc3}. (c) Current harmonic spectrum of $i_{\mathrm{in}}(t)$.

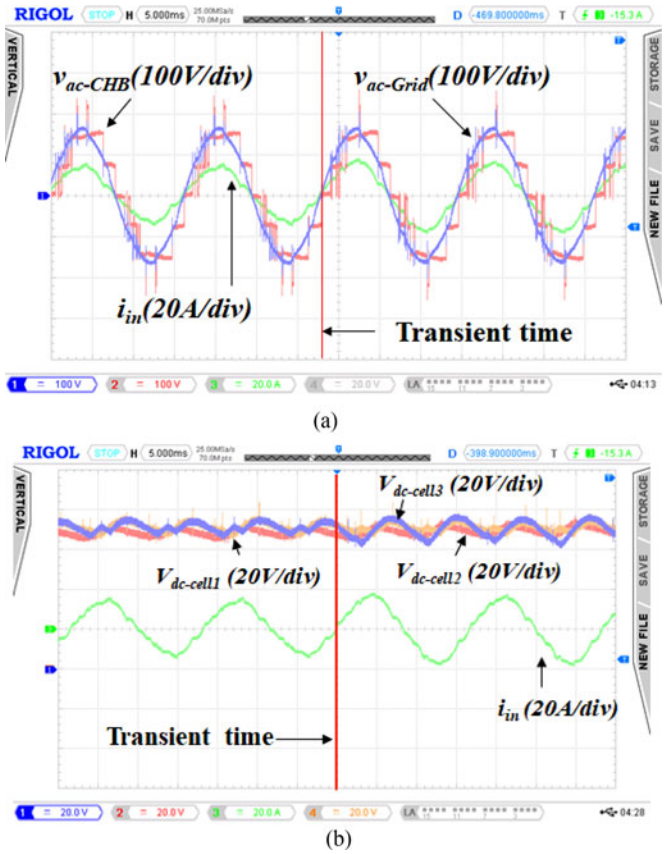

Fig. 13. Experimental result of the proposed sensor-less voltage balancing technique in transient condition when active power of cell 3 is changed from 326.67 (equal loads) to 515.25 W (unequal loads), and $V_{\rm dc} = 70$ V. (a) Time domain waveforms of $v_{\rm ac-CHB}(t)$, $v_{\rm ac-Grid}(t)$, and $i_{\rm in}(t)$. (b) Time domain waveforms of V_{dc1}, V_{dc2}, and V_{dc3}.

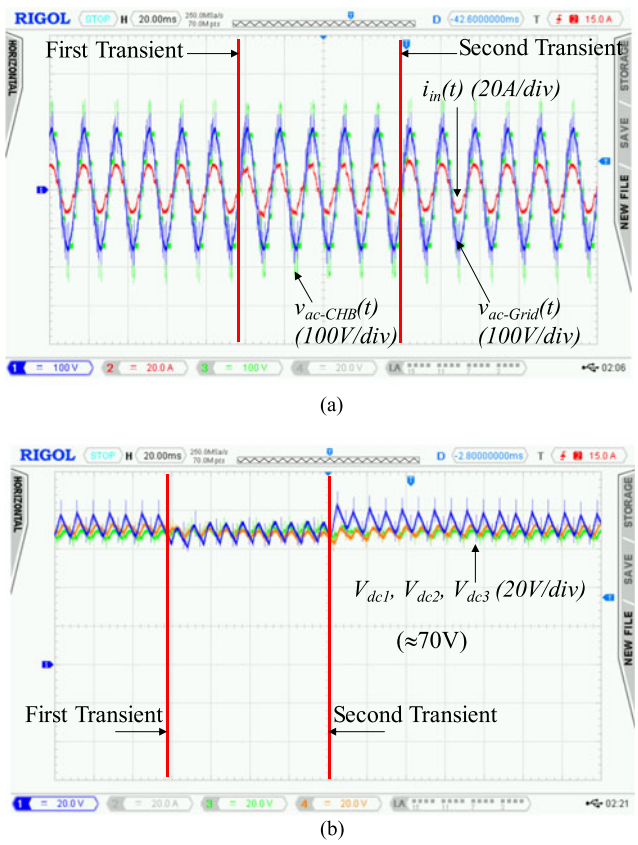

Fig. 14. Experimental result of the proposed sensor-less voltage balancing technique in dynamic condition when the active and reactive power changes from 1030 to 1030 W–375 VAr at first transient and returns to 1030 W at second transient at PCC. (a) Time domain waveforms of $v_{\rm ac-CHB}(t)$, $v_{\rm ac-Grid}(t)$, and $i_{\rm in}(t)$. (b) Time domain waveforms of V_{dc1}, V_{dc2}, and V_{dc3}.

harmonics in Fig. 12(c) are due to the accuracy of the switching angles in experiment. In the second experiment, the active power flowing through all of the dc loads is 980 W before the transient. Each cell has around 266.7 W. No reactive power is injected or absorbed from the power grid. At transient, the load of the third cell is increased by 57% from 326.67 to 515.25 W. The modulation index of converter is changed from 2.152 to 2.180 correspondingly. Fig. 13 shows the $v_{\rm ac-CHB}(t)$, $v_{\rm ac-Grid}(t)$, and $i_{\rm in}(t)$ for the proposed voltage balancing technique with ASHCM-PWM technique with equal (before transient) and unequal (after transient) loads. Fig. 13(a) shows the time domain waveforms. $i_{\rm in}(t)$ is in phase with $v_{\rm ac-Grid}(t)$. In Fig. 13(b), the dc link voltages of three cells are regulated to 70 V. The low frequency oscillation in Fig. 13(b) is due to the second-order harmonic ripple of ac power.

In the last experiment in Fig. 14, the dynamic performance of the proposed voltage balancing technique is tested. The active and reactive power changes from 1030 W to 1030 W–375 VAr at PCC for the first transient condition. Then, the power of CHB converter returns to 1030 W at the second transient in Fig. 14. The modulation index of converter is changed between 2.165 and 2.347 during the first transient condition. Fig. 14(a) shows the time domain waveforms of the proposed technique for $v_{\rm ac-CHB}(t)$, $v_{\rm ac-Grid}(t)$, and $i_{\rm in}(t)$. As discussed in [19] and shown in Fig. 10(a), ASHCM-PWM has a weak dynamic performance, so it generates a small dc term when the active and reactive power is changed. This is actually true for all low frequency modulation techniques. This issue can be solved by applying high-frequency PSPWM during the dynamic period [19]. As shown in Fig. 14(b), the dc link voltages of the grid-tied converter are balanced to be 70 V under the dynamic condition.

VI. Conclusion

In this paper, a sensor-less voltage balancing technique for grid-tied CHB converters with ASHCM-PWM technique was proposed. The proposed voltage balancing technique could control the dc link voltages without using expensive dc link sensors for equal and unequal loads. The proposed technique can mitigate the current harmonics of CHB converters to meet the current harmonic limits defined in the IEEE-519. In addition, the phase of input current is derived based on the parameters of the CHB converters and it can be used to determine the ranges of active and reactive power generated by the CHB converters. The proposed voltage balancing technique is very simple. It does not use any complex controllers to balance dc link voltages. This technique can also be simply implemented for three-phase grid-tied converters or STATCOM applications.

REFERENCES

[1] S. Khomfoi and L. M. Tolbert, "Multilevel power converters," in *Power Electronics Handbook*, 3rd ed. New York, NY, USA: Elsevier, 2011, pp. 455–486.

[2] M. S. A. Dahidah, G. Konstantinou, and V. G. Agelidis, "A review of multilevel selective harmonic elimination PWM: Formulations, solving algorithms, implementation and applications," *IEEE Trans. Power Electron.*, vol. 30, no. 8, pp. 4091–4106, Aug. 2015.

[3] F. Khoucha, S. M. Lagoun, K. Marouani, A. Kheloui, and M. E. H. Benbouzid, "Hybrid cascaded H-bridge multilevel inverter motor drive DTC control for electric vehicles," in *Proc. 2008 18th Int. Conf. Elect. Mach.*, Vilamoura, Portugal, 2008, pp. 1–6.

[4] T. Zhao, G. Wang, S. Bhattacharya, and A. Q. Huang, "Voltage and power balance control for a cascaded H-bridge converter-based Solid-State transformer," *IEEE Trans. Power Electron.*, vol. 28, no. 4, pp. 1523–1532, Apr. 2013.

[5] C. D. Townsend, T. J. Summers, and R. E. Betz, "Multigoal heuristic model predictive control technique applied to a cascaded H-bridge StatCom," *IEEE Trans. Power Electron.*, vol. 27, no. 3, pp. 1191–1200, Mar. 2012.

[6] S. Wang, R. Crosier, and Y. Chu, "Investigating the power architectures and circuit topologies for megawatt superfast electric vehicle charging stations with enhanced grid support functionality," in *Proc. Int. Conf. IEEE Elect. Veh.*, Greenville, SC, USA, 2012, pp. 1–8.

[7] A. Moeini, H. Iman-Eini, and A. Marzoughi, "DC link voltage balancing approach for cascaded H-bridge active rectifier based on selective harmonic elimination-pulse width modulation," *IET Power Electron.*, vol. 8, no. 4, pp. 583–590, 2015.

[8] A. Moeini, H. Zhao, and S. Wang, "A current reference based selective harmonic current mitigation PWM technique for cascaded H-bridge multilevel active rectifiers with small coupling inductance, extended harmonic reduction spectrum and the ability to reduce the harmonic currents due to grid voltage harmonics" *IEEE Trans. Ind. Electron.*, to be published, 2018 (early access). [Online]. Available: http://ieeexplore.ieee.org/abstract/document/7748491/

[9] M. Aleenejad, H. Mahmoudi, P. Moamaei, and R. Ahmadi, "A new fault-tolerant strategy based on a modified selective harmonic technique for three-phase multilevel converters with a single faulty cell," *IEEE Trans. Power Electron.*, vol. 31, no. 4, pp. 3141–3150, Apr. 2016.

[10] M. Dabbaghjamanesh, A. Moeini, M. Ashkaboosi, P. Khazaei, and K. Mirzapalangi, "High performance control of grid connected cascaded H-Bridge active rectifier based on type II-fuzzy logic controller with low frequency modulation technique," *Int. J. Electr. Comput. Eng.*, vol. 6, no. 2, pp. 484–94, Apr. 2016.

[11] L. G. Franquelo, J. Napoles, R. C. P. Guisado, J. I. Leon, and M. A. Aguirre, "A flexible selective harmonic mitigation technique to meet grid codes in three-level PWM rectifiers," *IEEE Trans. Ind. Electron.*, vol. 54, no. 6, pp. 3022–3029, Dec. 2007.

[12] A. Marzoughi, H. Imaneini, and A. Moeini, "An optimal selective harmonic mitigation technique for high power converters," *Int. J. Electr. Power Energy Syst.*, vol. 49, pp. 34–39, 2013.

[13] M. Najjar, A. Moeini, M. K. Bakhshizadeh, F. Blaabjerg, and S. Farhangi, "Optimal selective harmonic mitigation technique on variable DC link cascaded H-bridge converter to meet power quality standards," *IEEE J. Emerg. Sel. Topics Power Electron.*, vol. 4, no. 3, pp. 1107–1116, Sep. 2016.

[14] D. G. Holmes and T. A. Lipo, *Pulse Width Modulation for Power Converters: Principles and Practice*. New York, NY, USA: Wiley, 2003.

[15] A. Moeini, Z. Hui, and S. Wang, "High efficiency, hybrid selective harmonic elimination phase-shift PWM technique for cascaded H-bridge inverters to improve dynamic response and operate in complete normal modulation indices," in *Proc. 2016 Int. Conf. IEEE Appl. Power Electron.*, Long Beach, CA, USA, 2016, pp. 2019–2026.

[16] M. Aleenejad, H. Iman-Eini, and S. Farhangi, "Modified space vector modulation for fault-tolerant operation of multilevel cascaded H-bridge inverters," *IET Power Electron.*, vol. 6, no. 4, pp. 742–751, Apr. 2013.

[17] A. J. Watson, P. W. Wheeler, and J. C. Clare, "A complete harmonic elimination approach to DC link voltage balancing for a cascaded multilevel rectifier," *IEEE Trans. Ind. Electron.*, vol. 54, no. 6, pp. 2946–2953, Dec. 2007.

[18] IEEE Recommended Practice and Requirements for Harmonic Control in Electric Power Systems," IEEE Standard 519-2014 (Revision of IEEE Standard 519-1992), Jun. 11, 2014.

[19] A. Moeini, Z. Hui, and S. Wang, "Improve control to output dynamic response and extend modulation index range with hybrid selective harmonic current mitigation-PWM and phase-shift PWM for four-quadrant cascaded H-Bridge converters," *IEEE Trans. Ind. Electron.*, vol. 64, no. 9, pp. 6854–6863, Sep. 2017.

[20] A. J. Watson, P. W. Wheeler, and J. C. Clare, "A selective harmonic elimination system for restoring and equalising DC link voltages in a multilevel active rectifier," in *Proc. 2007 Eur. Conf. Power Electron. Appl.*, Aalborg, Denmark, 2007, pp. 1–7.

[21] M. K. Bakhshizadeh, M. Najjar, F. Blaabjerg, and R. Sajadi, "Using variable DC sources in order to improve the voltage quality of a multilevel STATCOM with low frequency modulation," in *Proc. 2016 18th Eur. Conf. Power Electron. Appl.*, Karlsruhe, Germany, 2016, pp. 1–10.

[22] A. Sanchez-Ruiz, G. Abad, I. Echeverria, I. Torre, and I. Atutxa, "Continuous phase-shifted selective harmonic elimination and DC-link voltage balance solution for H-bridge multilevel configurations, applied to 5L HNPC," *IEEE Trans. Power Electron.*, vol. 32, no. 4, pp. 2533–2545, Apr. 2017.

[23] M. S. A. Dahidah, V. G. Agelidis, and M. V. Rao, "On abolishing symmetry requirements in the formulation of a five-level selective harmonic elimination pulse-width modulation technique," *IEEE Trans. Power Electron.*, vol. 21, no. 6, pp. 1833–1837, Nov. 2006.

[24] H. Zhao and S. Wang, "A four-quadrant modulation technique to extend modulation index range for multilevel selective harmonic elimination/compensation using staircase waveforms," *IEEE J. Emerg. Sel. Topics Power Electron.*, vol. 5, no. 1, pp. 233–243, Mar. 2017.

[25] M. Reyes-Sierra and C. A. Coello Coello, "Multi-objective particle swarm optimizers: A survey of the state-of-the-art," *Int. J. Comput. Intell. Res.*, vol. 2, no. 3, pp. 287–308, 2006.

Amirhossein Moeini (S'16) received the B.Sc. degree in electrical engineering from the University of Guilan, Rasht, Iran, in 2011, and the M.Sc. degree in power electronics and electrical machines from the University of Tehran, Tehran, Iran, in 2013. He is currently working toward the Ph.D. degree in power electronics with Electrical Power Research Laboratory, University of Florida, Gainesville, FL, USA.

His current research interests include modeling and control of power electronic converters, FACTS devices, power quality, evolutionary optimization methods, and optimal modulation techniques.

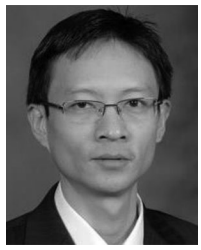

Shuo Wang (S'03–M'06–SM'07) received the Ph.D. degree in electrical engineering from Virginia Tech, Blacksburg, VA, USA, in 2005.

Since 2015, he has been an Associate Professor with the Department of Electrical and Computer Engineering, University of Florida, Gainesville, FL, USA. From 2010 to 2014, he was with the University of Texas at San Antonio, San Antonio, TX, USA, first as an Assistant Professor and later as an Associate Professor. From 2009 to 2010, he was a Senior Design Engineer in GE Aviation Systems, Vandalia, OH, USA. From 2005 to 2009, he was a Research Assistant Professor at Virginia Tech, Blacksburg, VA.

Dr. Wang has published more than 140 IEEE journal and conference papers and holds eight US patents. He was the recipient of the Best Transaction Paper Award from the IEEE Power Electronics Society in 2006 and two William M. Portnoy Awards for the papers published in the IEEE Industry Applications Society in 2004 and 2012, respectively. In 2012, he was the recipient of the prestigious National Science Foundation CAREER Award. He is an Associate Editor for the IEEE TRANSACTIONS ON INDUSTRY APPLICATIONS and a technical program Co-Chair for the IEEE 2014 International Electric Vehicle Conference.